Targeting negative energy balance with calorie restriction and mitochondrial uncoupling in db/db mice

Chen, Sing-Young; Beretta, Martina; Olzomer, Ellen M; Shah, Divya P; Wong, Derek Y H; Alexopoulos, Stephanie J

Published in:
Molecular Metabolism

DOI:
10.1016/j.molmet.2023.101684

Publication date:
2023

Original Article

MOLECULAR METABOLISM

Targeting negative energy balance with calorie restriction and mitochondrial uncoupling in *db/db* mice

Sing-Young Chen [1], Martina Beretta [1], Ellen M. Olzomer [1], Divya P. Shah [1], Derek Y.H. Wong [1], Stephanie J. Alexopoulos [1], Isabella Aleksovska [1], Joseph M. Salamoun [2], Christopher J. Garcia [2], Blake J. Cochran [3], Kerry-Anne Rye [3], Greg C. Smith [3], Frances L. Byrne [1], Margaret J. Morris [3], Webster L. Santos [2], James Cantley [4], Kyle L. Hoehn [1,*]

ABSTRACT

Objective: Calorie restriction is a first-line treatment for overweight individuals with metabolic impairments. However, few patients can adhere to long-term calorie restriction. An alternative approach to calorie restriction that also causes negative energy balance is mitochondrial uncoupling, which decreases the amount of energy that can be extracted from food. Herein we compare the metabolic effects of calorie restriction with the mitochondrial uncoupler BAM15 in the *db/db* mouse model of severe hyperglycemia, obesity, hypertriglyceridemia, and fatty liver.
Methods: Male *db/db* mice were treated with ~50% calorie restriction, BAM15 at two doses of 0.1% and 0.2% (*w/w*) admixed in diet, or 0.2% BAM15 with time-restricted feeding from 5 weeks of age. Mice were metabolically phenotyped over 4 weeks with assessment of key readouts including body weight, glucose tolerance, and liver steatosis. At termination, liver tissues were analysed by metabolomics and qPCR.
Results: Calorie restriction and high-dose 0.2% BAM15 decreased body weight to a similar extent, but mice treated with BAM15 had far better improvement in glucose control. High-dose BAM15 treatment completely normalized fasting glucose and glucose tolerance to levels similar to lean *db/+* control mice. Low-dose 0.1% BAM15 did not affect body mass but partially improved glucose tolerance to a similar degree as 50% calorie restriction. Both calorie restriction and high-dose BAM15 significantly improved hyperglucagonemia and liver and serum triglyceride levels. Combining high-dose BAM15 with time-restricted feeding to match the time that calorie restricted mice were fed resulted in the best metabolic phenotype most similar to lean *db/+* controls. BAM15-mediated improvements in glucose control were associated with decreased glucagon levels and decreased expression of enzymes involved in hepatic gluconeogenesis.
Conclusions: BAM15 and calorie restriction treatments improved most metabolic disease phenotypes in *db/db* mice. However, mice fed BAM15 had superior effects on glucose control compared to the calorie restricted group that consumed half as much food. Submaximal dosing with BAM15 demonstrated that its beneficial effects on glucose control are independent of weight loss. These data highlight the potential for mitochondrial uncoupler pharmacotherapies in the treatment of metabolic disease.

Keywords Calorie restriction; Mitochondrial uncoupling; Obesity; Diabetes

1. INTRODUCTION

Metabolic disease often manifests as multiple related comorbidities, including obesity, type 2 diabetes, and non-alcoholic fatty liver disease. For many decades, the prevalence of these diseases has continued to increase despite advances in management and treatment [1–3]. Chronic metabolic disease results in significant loss of quality of life and increases the risk of other illnesses, including cardiovascular disease [4], cancer [5], neurodegenerative disease [6], and severe COVID19 [7]. Therefore, the burden of metabolic disease on global healthcare systems is serious and likely to continue to worsen.
Frontline management of metabolic disease begins with lifestyle interventions including diet and exercise. Lifestyle interventions are low-cost and non-invasive but are limited by poor patient compliance and have failed to control the burden of metabolic disease in the long-term. While calorie restriction is initially highly effective for weight loss and improving metabolic outcomes, long-term calorie restriction results in undesired compensatory changes (e.g. decreased basal metabolic

[1]School of Biotechnology and Biomolecular Sciences, University of New South Wales, Sydney, NSW, 2052, Australia [2]Department of Chemistry and Virginia Tech Centre for Drug Discovery, Virginia Tech, Blacksburg, VA, 24061, USA [3]School of Biomedical Sciences, University of New South Wales, Sydney, NSW, 2052, Australia [4]School of Medicine, University of Dundee, Dundee DD1 4HN, UK

*Corresponding author. Biological Sciences North Building (D26), Upper Kensington Campus, University of New South Wales, Randwick, NSW, 2052, Australia. E-mail: k.hoehn@unsw.edu.au (K.L. Hoehn).

Received November 28, 2022 • Revision received January 23, 2023 • Accepted January 24, 2023 • Available online 31 January 2023

https://doi.org/10.1016/j.molmet.2023.101684

rate) that defend against further weight loss and counteract the effects of calorie restriction [8]. An alternative to decreasing nutrient intake is to decrease the efficiency of nutrient metabolism through mitochondrial uncoupling [9].

Mitochondrial uncoupler drugs work by decreasing the efficiency of mitochondrial ATP production so that more nutrients are metabolized to generate a given amount of ATP [10]. Therefore, mitochondrial uncoupling and calorie restriction both result in a net negative energy balance. Mitochondrial uncoupling also decreases mitochondrial superoxide production by decreasing electron leak from the mitochondrial respiratory chain [9], producing a similar effect as calorie restriction, which also has antioxidant effects and decreases oxidative damage [11,12]. Together, the dual effects of increased nutrient oxidation and decreased oxidative stress have potential clinical use for the treatment of disorders related to obesity and insulin resistance. To our knowledge, this is the first study where calorie restriction and mitochondrial uncoupling have been compared head-to-head in a mouse disease model.

Herein we compared the efficacy of BAM15 and ~50% calorie restriction in *db/db* mice. *Db/db* mice, which lack functional leptin receptor, suffer from obesity, hyperglycemia, hypertriglyceridemia, hyperglucagonemia, and liver steatosis by 9 weeks of age, while mice with one functional leptin receptor gene (*db/+*) are metabolically normal [13,14]. The 50% calorie restriction was achieved by providing *db/db* mice the same amount of food as was eaten by *db/+* lean controls. Previous studies have shown that a similar degree of calorie restriction has efficacy against weight gain, hyperglycemia, and hepatic steatosis in *db/db* mice [15,16], although blood glucagon levels were not assessed and hypertriglyceridemia was not significantly improved. Since calorie-restricted mice are given food once per day, they are subjected to time-restricted feeding. Therefore, we added another control group of mice that served two purposes: being given food once per day (at the same time as the calorie-restricted mice) and being fed the same amount of food as *db/db* control mice (pair-fed) to rule out potential for over-eating.

Overall, the results of this study showed that high-dose BAM15 treatment resulted in similar metabolic phenotypes as calorie restriction in the context of improving body weight, hypertriglyceridemia, hyperglucagonemia, and liver steatosis. However, high-dose BAM15 had far better effects to normalize glucose homeostasis. Low-dose BAM15 treatment improved glucose control without affecting body weight, thereby demonstrating that its effects were at least partially independent of weight loss. The combination of high-dose BAM15 with pair-feeding resulted in the best phenotype that was most similar to healthy *db/+* mice. Notably, the BAM15 treatments did not decrease food intake or decrease skeletal muscle mass. Metabolomic, biochemical, and gene expression studies further elucidate that BAM15 represses the expression of key rate-limiting enzymes in gluconeogenesis.

This is the first study to test BAM15 in the *db/db* mouse model. Therefore, as a benchmarking control for BAM15, we treated another group of mice with the only other mitochondrial uncoupler that is commercially available and shown to mildly improve metabolic phenotypes in *db/db* mice, niclosamide ethanolamine (NEN) [17]. Over the course of this study, we found that NEN was not effective at the dose (0.15% (*w/w*), 1500 ppm) previously published to improve glucose levels in *db/db* mice [17]. Therefore, our NEN data is consistent with work by Hinder and colleagues who were also unable to demonstrate efficacy with NEN treatment at this dose [18]. For clarity of readership, NEN data is not shown in the main figures and moved to the supplement.

2. MATERIALS AND METHODS

2.1. Cellular oxygen consumption assay

Oxygen consumption rate (OCR) was measured using an Agilent Seahorse XFe96 analyzer (Agilent Technologies, Santa Clara, CA). L6 myoblasts were seeded in a Seahorse tissue culture plate at a density of 2×10^4 cells/well and allowed to adhere overnight. Prior to the assay, the medium was changed to unbuffered DMEM (Sigma D5030, pH = 7.4 at 37 °C) supplemented with glucose (25 mM), sodium pyruvate (1 mM, Sigma S8636) and L-glutamine (4 mM, Sigma G7513) and the cells were equilibrated for 1 h at 37 °C without CO_2. In each well, a single concentration of BAM15 or NEN was injected during the assay in media containing DMSO such that the final DMSO concentration was 0.4%. OCR was measured using 3-minute measurement periods over 2 h following drug injection. The first three measurements after injection for each concentration were averaged to produce a dose—response curve. Data presented show n = 3 independent assays with 4 replicate wells per treatment.

2.2. Animal husbandry

All mouse experiments were conducted at UNSW and approved by the UNSW Animal Care and Ethics Committee (project approval 20/67 A). *Db/db* mice (BKS.Cg-Dock7^{m}+/+Lepr^{db}/J^{Ausb}) were obtained from an existing line and bred at Australian BioResources (Moss Vale, NSW, Australia) and were used as indicated. Mice were housed in specific pathogen-free conditions at 22 °C with a light/dark cycle of 12 h. Mice were housed in groups of up to 5 littermates prior to treatment, at which point *db/db* mice were single-housed and *db/+* mice were group-housed where possible, depending on the litters from which they originated. Mice were monitored as per ethical guidelines, including body weight measurements as described below. Unless otherwise stated, mice were provided with *ad libitum* access to water and standard chow diet (Gordons Specialty Feeds, NSW, Australia).

2.3. Indirect calorimetry

Indirect calorimetry was performed using an Oxymax CLAMS (Columbus Instruments' Comprehensive Lab Animal Monitoring System, USA) indirect calorimeter in the Biological Resource Centre at UNSW. 12-week-old *db/db* mice were allowed to acclimatize for at least 24 h prior to data collection. Mice were stratified into vehicle or BAM15 groups based on lean body mass. To test the effect of an oral bolus, vehicle or 100 mg/kg BAM15 was administered by oral gavage in a formulation containing 0.7% methylcellulose (Sigma M0512, 93%), Tween80 (Sigma P6474, 2%) and DMSO (Sigma D5879, 5%). These mice were fed powdered chow food *ad libitum*. For indirect calorimetry of mice fed BAM15 admixed in food, measurements were taken on day 3 of treatment with pellets of normal chow or chow containing 0.2% (*w/w*) BAM15, prepared in-house as described below. Oxygen consumption and carbon dioxide output were normalized to lean mass as assessed by EchoMRI. Respiratory exchange ratio (RER) was calculated as the ratio of carbon dioxide output over oxygen consumption.

2.4. Preparation of animal diets

Chow diets containing drug were prepared by first powdering normal chow diet using a food processor. Powdered diet was mixed with the correct concentration of BAM15 (obtained from Santos Lab, Virginia Tech, U.S.A.) or niclosamide ethanolamine (NEN) (Nanjing Chemlin Chemical Industry Co., Ltd., China) and compressed into pellets using a pellet mill (Gemco ZLSP-120 B). For untreated chow diet, powdered diet was pressed into pellets without adding any drug.

2.5. Overnight body temperature measurement

8-week-old male *db/db* mice were stratified into three groups based on body weight and randomly assigned to chow or chow containing 0.2% (*w/w*) BAM15. A group of *db/+* littermates were included as lean controls. After a 6-day run-in period, mice were monitored over 24 h with body temperature measured every 3 h using a rectal probe thermometer (Braintree TW2-107). At this time, a small amount of blood (~15 μL) was collected in heparinized capillary tubes (Sarstedt 16.443). Plasma was extracted by centrifugation at 4 °C and 2000×*g* for 10 min and processed for LC-MS/MS analysis for drug concentrations as described below.

2.6. LC-MS/MS determination of drug concentration

To process plasma for LC-MS/MS analysis, 7 μL of plasma was added to 100 μL of an acetonitrile: methanol mixture (9:1), vortexed and centrifuged at 21 130×*g* for 10 min at 4 °C, and the supernatant collected into autosampler vials for analysis. Standards were prepared by spiking known amounts of BAM15 into untreated plasma. LC-MS/MS was conducted on a Shimadzu Prominence LCMS-8030 as previously described [19], using a transition of *m/z* 341 > 162 and a retention time of 6 min in positive mode for BAM15.

2.7. Study design

To obtain baseline measurements, male *db/+* and *db/db* mice were assessed for glucose tolerance at 5–6 weeks of age. *Db/db* mice were stratified into treatment groups, as follows. Four groups of *db/db* mice were fed *ad libitum*: chow (control), chow with 0.1% (*w/w*) BAM15, chow with 0.2% (*w/w*) BAM15 and chow with 0.15% (*w/w*) NEN. Another group of *db/db* mice were pair-fed untreated chow to receive the same average food intake as *db/+* mice as a model of calorie restriction (*db/db* CR). Unfortunately, food intake in *db/db* mice fed 0.2% BAM15 was difficult to measure accurately due to a high quantity of pulverized food at the bottom of the cage. Therefore, to better control for food intake, as well as the time-restricted feeding displayed by the CR group, a final group of *db/db* mice were given the higher dose of BAM15 (0.2%) in the same quantity (8 g) as chow-fed *db/db* mice, at the same time as the CR mice were fed. These mice were observed to consume all food provided each day and are referred to as *db/db* pair-fed (PF) 0.2% BAM15. Furthermore, a separate cohort of mice (n = 7–8 per group) was given chow or 0.2% BAM15 *ad libitum* for a more intensive food monitoring study involving the collection of powdered food. Food traps were placed beneath hoppers and any leftover food was separated from droppings as much as possible and weighed daily. Food remaining in the hopper was also weighed daily.

At the end of the 4-week treatment period, a glucose tolerance test was conducted. At termination, serum was collected by taking blood via cardiac puncture under isoflurane anesthesia. Blood was kept on ice before being centrifuged at 2000×*g* and 4 °C for 10 min to extract serum. Mice were euthanized by cervical dislocation and harvested tissues were frozen in liquid nitrogen and stored at −80 °C.

2.8. Glucose tolerance test

Mice received intraperitoneal injections of 20% (*w/v*) dextrose at a dose of 1 g/kg lean body mass following a 6-hour daytime fast. Blood glucose was monitored at regular intervals using an Accuchek Performa glucometer. As the upper limit of the glucometer is 33.3 mM, readings above 33.3 mM (HI) were recorded as 33.3 mM. The total area under the curve was calculated using the trapezoidal method.

2.9. Plasma insulin and serum C-peptide, proinsulin, and glucagon measurements

Blood (~40 uL) was collected from the tail tip in heparinized capillary tubes (Sarstedt 16.443) in the random fed state (AM) and after a 6-hour daytime fast (PM). Plasma was extracted following centrifugation at 2000×*g* and 4 °C for 10 min. Plasma insulin was measured using a Crystal Chem Ultra-Sensitive Mouse Insulin ELISA Kit (Crystal Chem Inc. 90080, Chicago, IL, USA) according to manufacturer's instructions except that test samples and standards were incubated overnight at 4 °C. For C-peptide measurements, terminal serum was analysed using a Crystal Chem Mouse C-peptide ELISA Kit (Crystal Chem Inc. 90050, Chicago, IL, USA) according to the manufacturer's instructions. For proinsulin measurements, terminal serum was analysed using a Mercodia Rat/Mouse Proinsulin ELISA Kit (Mercodia AB 10-1232-01, Uppsala, Sweden) according to the manufacturer's instructions. For glucagon measurements, terminal serum was analysed using a Crystal Chem Mouse Glucagon ELISA Kit (Crystal Chem Inc. 81518, Chicago, IL, USA) according to the manufacturer's instructions.

2.10. HOMA-IR (homeostatic model assessment for insulin resistance)

The HOMA-IR index was calculated from fasting glucose and fasting insulin concentrations using the equation:

$$\text{HOMA} - \text{IR} = \frac{\text{Fasting glucose (mM)} \times \text{Fasting insulin (}\mu\text{IU/L)}}{22.5}$$

To convert insulin concentration from ng/mL into μIU/L, a molar mass of 5808 Da and a conversion factor of 1 μIU/L = 6.00 pmol/L were used.

2.11. Hepatic lipid content

Frozen liver tissue was powdered in liquid nitrogen using a tissue pulverizer (Cellcrusher, Cork, Ireland). Lipids were extracted using a modified version of the Folch method [20]. In brief, 25 mg of frozen powdered tissue was weighed out and vortexed in 533 μL chloroform and 267 μL methanol. Samples were sonicated for 10 min then digested on a rocker at room temperature for 45 min. 400 μL of 0.9% sodium chloride was added and samples were vortexed before centrifugation at 600×*g* at room temperature for 10 min. The bottom layer was extracted and dried under nitrogen gas in a TurboVap® Evaporator (Biotage, Uppsala, Sweden). Lipids were resuspended in 0.4 mL 95% (*v/v*) ethanol and heated to 37 °C prior to lipid assays. Triglyceride levels were measured by a colorimetric assay through reaction with GPO reagent (Pointe Scientific T7532, Canton, MI, USA) according to the manufacturer's protocol, using glycerol standard (Sigma G7793, St Louis, MO, USA).

2.12. Liver glycogen measurement

25 mg of powdered frozen liver tissue was weighed out and digested in 300 μL 0.5 mol L^{-1} potassium hydroxide for 30 min at room temperature. Then, 25 μL of saturated sodium sulfate and 750 μL of 100% methanol were added and samples were incubated at −80 °C for 1 h. Following this, glycogen was pelleted by centrifugation at 11 337×*g* at 4 °C for 5 min and the supernatant was discarded. 2 mg/mL amyloglucosidase solution was prepared by dissolving amyloglucosidase (Sigma 10115) in sodium acetate buffer (0.25 mol L^{-1}, pH 4.75). 200 μL of amyloglucosidase solution was added to each glycogen

sample and mixed well. Samples were incubated at 37 °C for 1 h prior to glucose assay.

Concentrations of liberated glucose were measured by colorimetric assay. Samples and glucose standards were incubated in freshly prepared reaction buffer (0.5 mg/mL 4-aminoantipyrine, 1.6 U/mL peroxidase, 10 U/mL glucose oxidase, and 1 g/L phenol in 0.12 mol L^{-1} phosphate buffer, pH 7) for 30 min at 37 °C in a 96-well microplate. Absorbance was read at 490 nm using a PerkinElmer EnSight® Plate Reader.

2.13. Histology and immunostaining

At termination, the left lobe of the liver and the tail of the pancreas were fixed in 10% formalin at room temperature overnight, then transferred to 70% ethanol and stored at 4 °C until processing. Sample processing and staining was performed by the Biological Specimen Preparation facility at the Mark Wainwright Analytical Centre, UNSW Sydney. Samples were embedded in paraffin and 4 μm sections were cut using a microtome. Immediately prior to staining, slides were dewaxed by baking for 60 min at 58 °C then put through a xylene/ethanol series.

For hematoxylin-eosin (H&E) staining, slides were stained in Harris hematoxylin for 5 min, then rinsed in tap water, Scott's solution, and tap water again. Slides were then dipped in 0.5% acid alcohol, rinsed in tap water, Scott's solution, and tap water once more, and then stained with eosin for 4 min. Slides were finally dehydrated and mounted.

For immunohistochemistry, rehydrated slides were subjected to antigen retrieval in citrate buffer (pH 6) in a pressure cooker at 110 °C for 5 min. After cooling for 20 min at room temperature, slides were washed in tris-buffered saline (TBS, DAKO), incubated in 3% H_2O_2 (Leica) to quench endogenous peroxidases, rinsed again in TBS, then incubated in primary antibody (anti-insulin 1:400 (Cell Signaling 4590) or anti-glucagon 1:200 (Cell Signaling 2760)) for 60 min at room temperature. Slides were then washed again in TBS, incubated in BOND polymer (Leica) for 8 min and washed again in TBS followed by distilled water. DAB reagent (Leica) was then applied for 10 min. Slides were rinsed in distilled water before counterstaining with hematoxylin (Leica), after which slides were washed again with distilled water, then TBS, then distilled water again. Finally, slides were dehydrated and mounted.

For immunofluorescence, staining was performed in the same way as DAB staining until after the antigen retrieval step. Then, slides were blocked with 0.1 M glycine in TBS for 30 min, rinsed with TBS, and incubated with primary antibody for 60 min at room temperature. Primary antibodies included: guinea pig anti-insulin (1:100, Bio-Rad 5330-0104G), mouse anti-glucagon (1:1000, Merck G2654) and rabbit anti-Ki67 (1:4000, Abcam 15580). After rinsing again with TBS, slides were incubated with a fluorescent secondary antibody for 30 min at room temperature. Secondary antibodies included: anti-guinea pig IgG Alexa549 (1:200, Thermofisher A11076), anti-mouse IgG Alexa488 (1:200, Thermofisher A32723) and anti-rabbit IgG Cy5 (1:200, Jackson 711-175-152). After secondary antibody incubation, slides were rinsed with TBS, then incubated in DAPI (2 μg/mL) for 5 min. Finally, slides were rinsed in TBS then distilled water, and coverslips were mounted using Prolong Mounting Medium (Thermofisher). Slides were stored at 4 °C until imaging.

Microscope images were acquired for all stained slides using an Olympus VS200 Slide Scanner with a magnification of 20×. Analysis of immunohistochemistry images was conducted in ImageJ. Scanned images showing the full section were first converted to RGB then deconvoluted using "H DAB". The same arbitrary threshold was set for all images, and DAB^+ and $hematoxylin^+$ areas were obtained. Analysis of immunofluorescence images was conducted using the cell counting function in QuPath. Insulin-positive, glucagon-positive and Ki67-positive cells were manually categorized and counted.

2.14. Metabolomics

Metabolomics was performed by Metabolomics Australia using both GC- and LC-MS techniques. Labelled internal standards were applied and pooled biological quality control samples were injected at regular intervals.

The protein contents of the pellets were determined by BCA assay using the Pierce BCA Assay Kit (Thermofisher) according to the manufacturer's protocol. Raw metabolomics data were extracted, peak-identified and QC-processed by Metabolomics Australia. Peak area under the curve (AUC) was first normalized to protein content then log_2-transformed for analysis.

2.15. Real-time quantitative PCR

RNA was extracted from powdered frozen mouse liver tissue using TRI Reagent (Sigma T9424). In brief, ~30 mg of frozen tissue was homogenized in 1 mL of TRI reagent using a pellet pestle homogenizer (Sigma Z359971). 300 μL of chloroform (Sigma C2432) was added and samples were vortexed for 30 s. Samples were spun at 12,000×*g* for 15 min at 4 °C and the upper aqueous layer was transferred to new tubes. 300 μL of isopropanol was added and samples were mixed and allowed to rest at room temperature for 10 min. RNA was then pelleted by centrifugation at 12,000×*g* for 10 min at 4 °C. RNA pellets were washed twice in 75% ethanol (Sigma E7023) and once in 95% ethanol, centrifuging at 7500×*g* for 10 min at 4 °C between washes. Pellets were air-dried and resuspended in nuclease-free water. Concentration was assessed using an Eppendorf BioSpectrometer.

cDNA was prepared with 1000 ng of RNA using the High-Capacity cDNA Reverse Transcription Kit (Thermofisher) according to the manufacturer's instructions. Quantitative real-time PCR (qRT-PCR) analysis was conducted using the following primers: *Ppia* (F: CGA TGA CGA GCC CTT GG, R: TCT GCT GTC TTT GGA ACT TTG TC), *Fbp1* (F: TCA ACT GCT TCA TGC TGG AC, R: GGG TCA AAG TCC TTG GCA TA), and *G6pc* (F: CCG GAT CTA CCT TGC TGC TCA CTT T, R: TAG CAG GTA GAA TCC AAG CGC GAA AC).

PCR products were amplified in the following 15 μL reaction on a 96-well plate: 667 nM primers, 7.5 μL iTaq Universal SYBR Green Supermix (Bio-Rad), 3.5 μL nuclease-free water, and 2 μL cDNA, or the following 10 μL reaction on a 384-well plate: 667 nM primers, 5 μL iTaq Universal SYBR Green Supermix (Bio-Rad), 2.67 μL nuclease-free water, and 1 μL cDNA. The housekeeping gene (*Ppia*) was included on every plate. The ViiA7 Real-Time PCR System (Applied Biosystems) was used with cycling conditions as follows: 95 °C (20 s), 40 cycles [95 °C (1 s) and 60 °C (20 s)] and melt curve stage [95 °C (15 s), 60 °C (1 min), and 95 °C (15 s)]. Quantification of gene expression was analysed as previously described [21].

2.16. Statistical analyses

All data points were collected from discrete biological replicates and are presented as the mean ± SEM. For glucose tolerance testing, data points were excluded from mice that did not receive a successful i. p. injection of glucose which included one mouse in the *db/db* CR group at baseline. In the indirect calorimetry experiment, one mouse was excluded due to extreme fluctuations in RER observed even before the oral gavage, which indicated a technical problem. For serum proinsulin measurements, one mouse from the *db/db* PF 0.2% BAM15 group was not included as its

absorbance was consistently lower than that of the lowest standard. In the immunohistochemistry data for islet glucagon, one sample from the *db/db* control group was excluded due to contamination during the staining process leading to false exaggeration of brown staining. For gene expression data, statistical outliers were identified and excluded by Grubbs' method [22] using Prism (v.8.4.2; GraphPad Software). For quadriceps weight, results were inadvertently not collected in 2 *db/+*, 1 *db/db* control, and 2 *db/db* 0.2% BAM15 mice. Sample size was determined using G*Power (v.3.1.9.7) with 80% power and 5% alpha with GTT-AUC as the primary outcome.

Statistical tests were conducted to determine differences between treatments groups. All groups were compared to *db/db* controls, unless otherwise specified. For normally distributed data, groups were compared by Student's t-test for two groups or One-Way ANOVA with Dunnett's correction for three or more groups, unless otherwise specified. The Welch's version of each test was used for unequal variance. For non-parametric data, the Mann-Whitney test was applied when comparing two groups and the Kruskal-Wallis test was undertaken for three or more groups with Dunn's multiple comparisons test. For multiple groups measured over time, analysis was performed by Two-Way Repeated Measures ANOVA with Dunnett's correction. Significance was determined to be reached when $p < 0.05$ using Prism (v.8.4.2, GraphPad Software).

3. RESULTS

3.1. BAM15 increased oxygen consumption in *db/db* mice

To determine the *in vivo* bioactivity of BAM15 in *db/db* mice, we first assessed the effect of BAM15 on energy expenditure using indirect calorimetry. Mice were treated with a bolus oral dose of 100 mg/kg body weight BAM15 or vehicle (Figure 1). Over the following 3 h, BAM15 treatment increased oxygen consumption (VO_2), which is a proxy for energy expenditure (Figure 1A). The respiratory exchange ratio (RER) was not significantly altered, although there was a trend for decreased RER in BAM15-treated mice (Figure 1B). The RER is a measure of the proportion of macronutrients being oxidized; a lower RER indicates greater fat oxidation. BAM15 did not increase locomotor activity, which suggests that its effect on energy expenditure is on-target mitochondrial respiration rather than secondary to increased physical activity (Figure 1C). We next investigated indirect calorimetry in mice consuming BAM15 *ad libitum* in chow diet at 0.2% (*w/w*) and observed a significant decrease in RER without a significant change in VO_2 (Fig. S2). One possible reason for the discrepancy between the routes of delivery could be that slow delivery of BAM15 in food over hours may result in VO_2 changes that are too small to resolve over baseline in free-moving mice; nevertheless, these results evidence the *in vivo* bioactivity of BAM15 in *db/db* mice.

For subsequent *in vivo* studies, BAM15 was administered admixed in food, rather than by oral gavage to minimize disturbance to animals and avoid any potential influence of the vehicle control (methylcellulose/Tween80/DMSO). As body temperature is an important safety marker with respect to mitochondrial uncouplers, we first assessed the effect of BAM15 feeding on body temperature in male *db/db* mice. Mice were provided with standard chow diet (control) or chow containing 0.2% (*w/w*) BAM15 and monitored over a 24-hour period. A group of lean heterozygous *db/+* mice were included as controls.

During this time, plasma BAM15 concentrations ranged from 0.6 to 1.8 μM with an average of 1.1 ± 0.14 μM (Fig. S1A), which is in the bioactive range for BAM15 and corresponds to ~2.6 times the EC_{50} of 0.42 μM [23]. Core body temperature was not significantly different between the *db/db* groups at any time point during the 24-hour measurement period (Fig. S1B).

3.2. High-dose BAM15 prevented weight gain to a similar extent as calorie restriction

To assess the effect of BAM15 treatment on metabolic health in *db/db* mice, we investigated seven groups of mice. Five groups were fed *ad libitum*, including *db/+* mice fed normal chow diet (lean control), *db/db* mice fed normal chow diet (*db/db* control), *db/db* mice fed BAM15 at 0.1% or 0.2% (*w/w*) admixed in chow diet, and *db/db* mice fed NEN at 0.15% (*w/w*) admixed in chow diet. Two groups underwent restricted feeding regimes. One of these was the calorie restriction (CR) group, which consisted of *db/db* mice fed the same amount of food as *db/+* mice that resulted in ~50% lower food intake. The addition of 0.1% BAM15 to food over a period of 4 weeks did not alter food intake in *db/db* mice (Fig. S3A), but we observed that *db/db* mice fed 0.2% BAM15 tended to shred the custom diet and spread it through the cage more than other groups, making it difficult to measure food intake for this specific group. Therefore, food intake behavior was also measured in a separate cohort of mice using a more labor-intensive monitoring method involving food traps, which demonstrated that 0.2% BAM15 admixed in food did not affect *ad libitum* food intake (Fig. S3B). We also included a sixth group where we provided mice with only the same amount of 0.2% (*w/w*) BAM15 diet as the average quantity of food consumed by untreated *db/db* mice fed chow diet *ad libitum* (referred to as pair-fed (PF) 0.2% BAM15). The pair-fed 0.2% BAM15 group were given food once per day at the same time as the calorie-restricted group. A final group was also included, consisting of *db/db* mice fed 0.15% NEN, a mitochondrial uncoupler that has previously shown efficacy *in vivo* in *db/db* mice [17]. The NEN compound used was confirmed to be biologically active by Seahorse oxygen consumption assays in L6 myoblasts (Fig. S4); however, NEN had negligible efficacy (supplementary materials).

As expected, after four weeks, *db/db* control mice had the highest body weights, at approximately 1.7 times that of *db/+* lean controls (Figure 2A). Compared to *db/db* controls, the calorie-restricted (CR) *db/db* mice had ~24% lower final body weight but were still 25% heavier than *db/+* mice (Figure 2A). The higher dose of 0.2% BAM15 fed *ad libitum* prevented body weight gain to a similar extent as CR, with these mice also being ~24% lighter than *db/db* controls (Figure 2A). Mice pair-fed 0.2% BAM15 to *db/db* controls showed the greatest prevention in body weight gain, with 36% less body mass compared to *db/db* controls despite identical food intake (Figures 2A, S3B). The mice given the lower dose of 0.1% BAM15 gained weight to a similar extent as *db/db* controls (Figure 2A).

At termination, we measured the masses of adipose, liver, and muscle tissues. The gonadal fat pad masses were significantly ($p < 0.05$) decreased by pair-feeding 0.2% BAM15 and CR, modestly but non-significantly decreased by 0.2% BAM15 *ad libitum*, and statistically unchanged by 0.1% BAM15 (Figure 2B). Inguinal fat mass was statistically lower in mice pair-fed 0.2% BAM15 compared to *db/db* controls, and non-significantly decreased by CR and 0.2% BAM15 *ad libitum* (Figure 2B). We also assessed the weight of dissected liver and quadriceps muscle at termination to better understand how treatment interventions affected lean tissue mass. Liver wet weight was more than twice as high in *db/db* control mice as in *db/+* mice (Figure 2C). Interventions that decreased liver weight compared to *db/db* control included CR (34% decrease), 0.2% BAM15 *ad libitum* (43% decrease) and 0.2% BAM15 pair-feeding (51% decrease) (Figure 2C). All *db/db* mice had smaller quadriceps muscles than *db/+* mice, but none of the treatment groups had decreased absolute quadriceps wet weight compared to the *db/db* controls (Figure 2D). NEN produced no changes in body weight or tissue masses compared to *db/db* controls, except for a mild (14%) decrease in liver weight (Fig. S5).

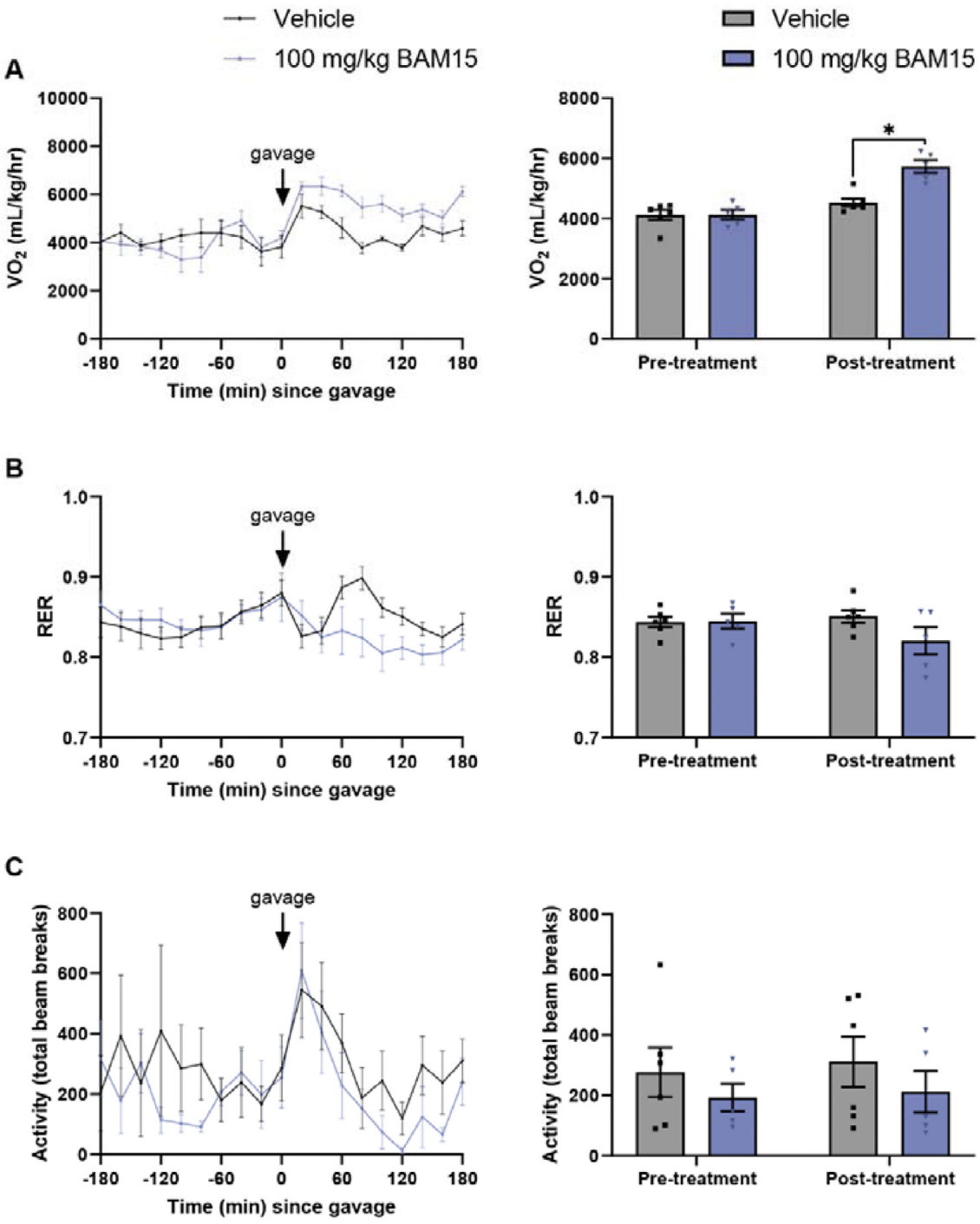

Figure 1: BAM15 administration increased oxygen consumption in *db/db* mice. Indirect calorimetry was conducted in *db/db* mice following an oral gavage of vehicle (grey) or BAM15 at 100 mg/kg body weight (blue). Oxygen consumption rate normalized to lean body mass (A). Respiratory exchange ratio (RER) calculated as the ratio of carbon dioxide output over oxygen consumption (B). Locomotor activity as the total number of laser beam breaks (C). Summary data indicate values averaged over 180 min pre- and post-gavage. * indicates $p < 0.05$ as assessed by Two-Way ANOVA with Sidak's correction. Graphs show mean ± SEM. n = 5–6 per group.

3.3. BAM15 produced greater improvements in glucose tolerance than calorie restriction

To assess the effect of treatment interventions on glucose homeostasis, glucose tolerance tests (GTTs) were conducted following a 6-hour daytime fast at two time points: one prior to starting treatment (pre-treatment) and one after 4 weeks of treatment (post-treatment). Blood glucose was measured at the time of fasting (AM) to represent a random-fed state and then measured again just prior to the commencement of the glucose tolerance test (PM) to assess the 6-hour fasting state.

All mice were administered glucose at a dose of 1 g/kg lean body mass and the resulting GTT curves showed considerable impairment in glucose tolerance in *db/db* controls compared to *db/+* mice (Figure 3A), which is also demonstrated in the increased total area

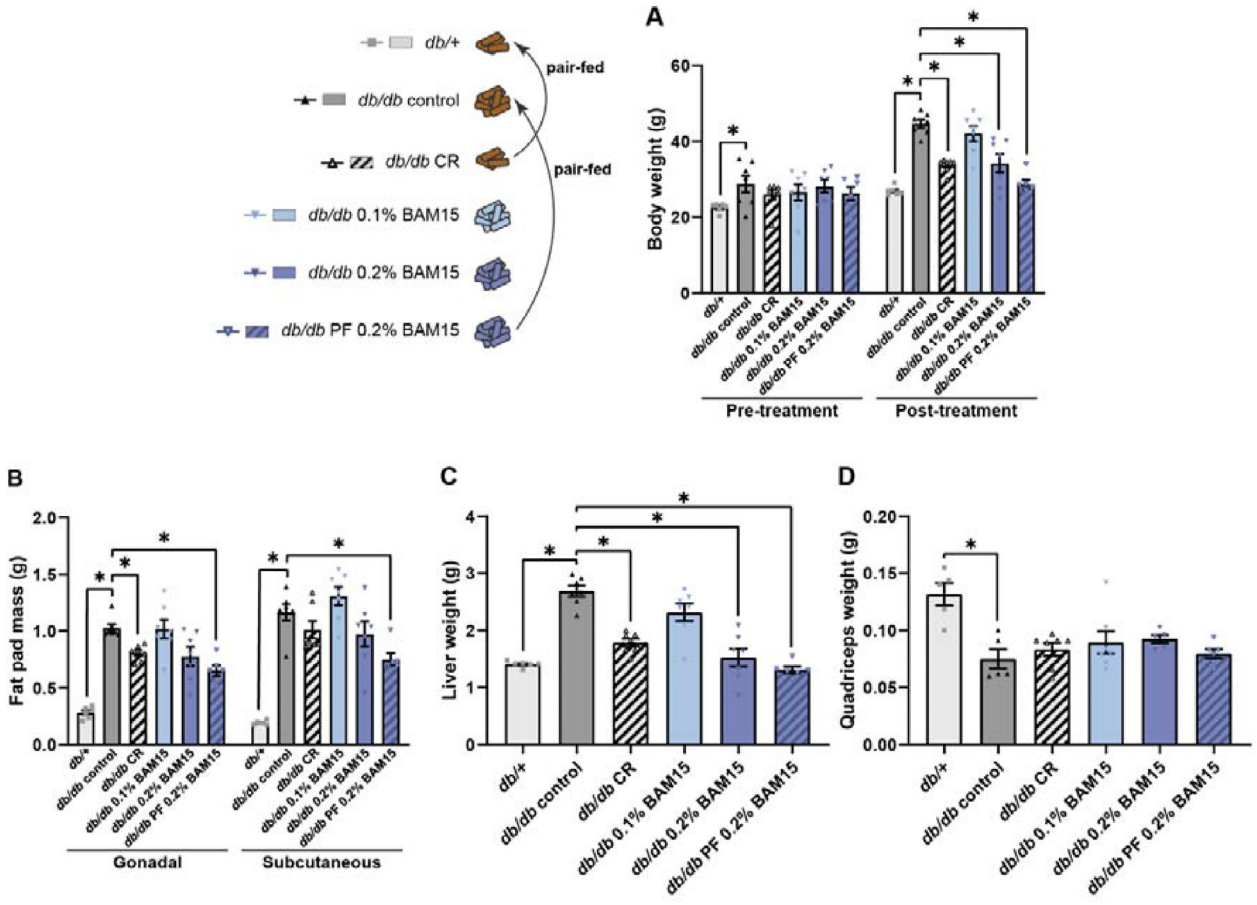

Figure 2: Calorie restriction and BAM15 treatments decreased body weight in *db/db* mice. *Db/db* mice were treated with BAM15 or calorie restricted for 4 weeks and body mass and tissue weights were measured. Body weights (A). Wet weights of fat pads (B), liver (C) and quadriceps muscle (D). * indicates $p < 0.05$ as assessed by Two-Way ANOVA (A) or One-Way ANOVA (B–D). All groups were compared to *db/db* controls. Graphs show mean ± SEM. n = 6–7 mice per group, except for quadriceps weight with n = 4–7 per group.

under the curve (Figure 3B). Mice fed 0.1% BAM15 in chow had markedly improved glucose tolerance, as well as lower fed and fasted glucose levels compared to *db/db* controls (Figure 3A–C) despite no improvement in body weight (Figure 2A). Glucose tolerance was very similar in mice fed 0.1% BAM15 and CR-treated mice, even though the calorie restricted mice consumed ~50% less food (Fig. S3) and weighed 20% less (Figure 2A).

Mice fed 0.2% BAM15 *ad libitum* showed remarkably similar glucose tolerance and fed and fasted glucose levels compared to lean *db/+* controls (Figure 3A–C) despite having greater body weight (Figure 2A). This dose of 0.2% BAM15 was sufficient to completely prevent the impairment in glucose tolerance and hyperglycemia observed in *db/db* control mice, achieving greater improvements than the 50% CR group (Figure 3A–C). Similar to the *db/db* mice fed 0.2% BAM15 *ad libitum*, the *db/db* mice pair-fed 0.2% BAM15 had glucose tolerance and blood glucose levels that were similar to lean, healthy *db/+* control mice (Figure 3A–C). Differences in glucose tolerance caused by BAM15 were largely independent of body weight; when GTT-AUC was graphed as a function of body weight, the slopes of fitted lines were relatively flat, and both doses of BAM15 resulted in lines that were non-intersecting and shifted downwards compared to *db/db* controls (Fig. S6). Mice fed NEN did not have lower fed or fasted glucose levels and remained hyperglycemic in the GTT to a similar extent as *db/db* control mice (Fig. S7).

3.4. BAM15 altered insulin and glucagon concentrations but not beta- and alpha-cell mass

Random-fed and fasted plasma insulin levels were similar among *db/db* mice. The only statistically significant change was an increase in fed insulin levels in the 0.1% BAM15 group (Figure 3D). Notably, the effect of BAM15 on insulin was not dose-dependent as 0.2% BAM15 did not affect insulin levels. However, C-peptide, which is co-secreted with insulin and has a longer half-life, was decreased by 0.2% BAM15 but not CR or 0.1% BAM15 in serum collected at termination (Figure 3E). Proinsulin levels, the elevation of which indicates dysfunctional insulin processing and secretion, were also decreased by both modes of 0.2% BAM15 feeding, compared to *db/db* controls (Figure 3F). In contrast, neither CR nor 0.1% BAM15 decreased circulating proinsulin (Figure 3F).

Fasting glucose and insulin concentrations were used to calculate HOMA-IR as an estimate of insulin resistance. After 4 weeks of treatment, HOMA-IR was increased in *db/db* controls compared to *db/+* mice and significantly decreased in both 0.2% BAM15 treatment groups (Figure 3G). Calorie-restricted mice showed a trend for decreased HOMA-IR compared to *db/db* controls (Figure 3G). Mice fed 0.1% BAM15 had elevated HOMA-IR (Figure 3G) due to higher insulin levels despite lower blood glucose (Figure 3C–D) compared to *db/db* controls.

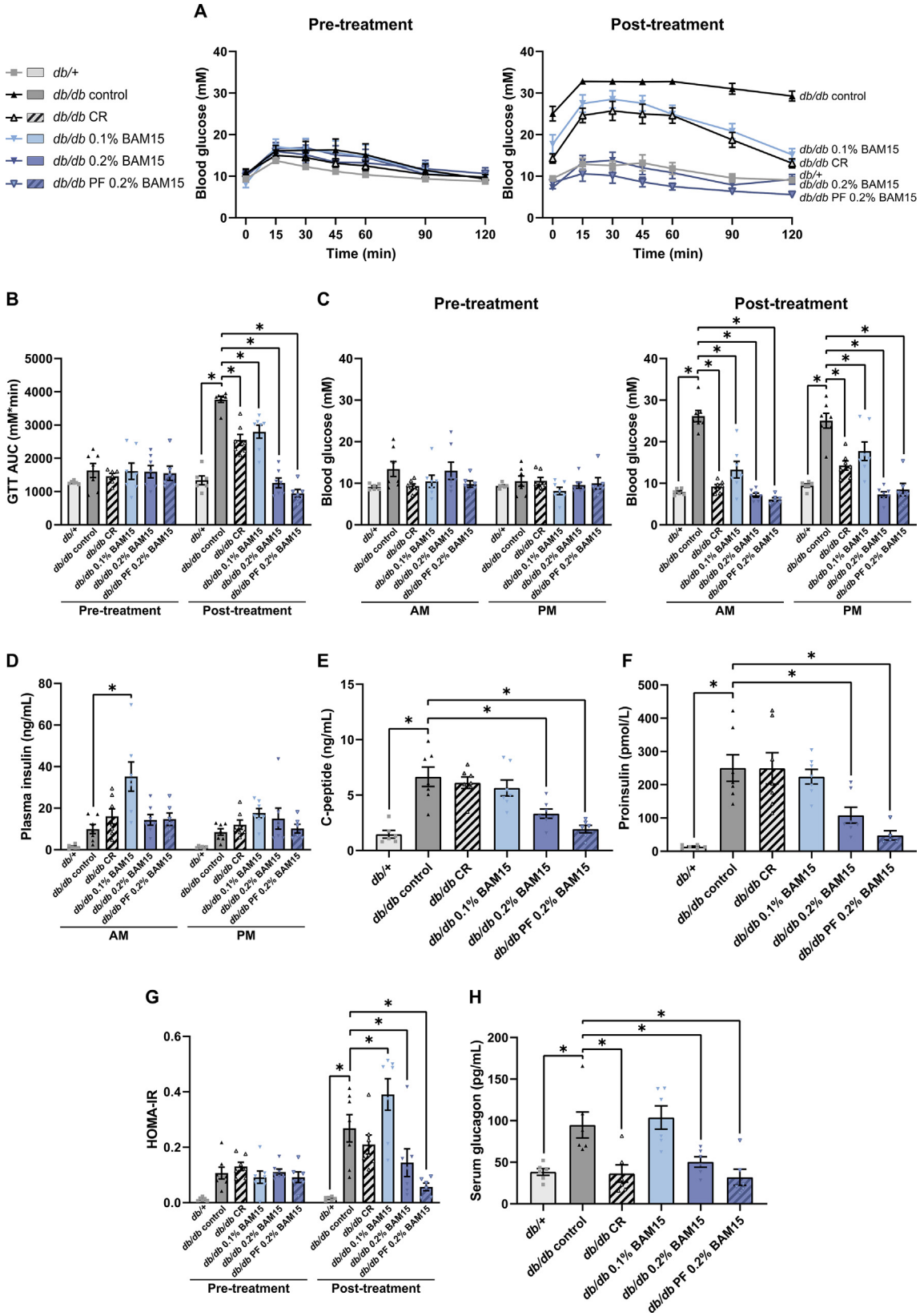

Figure 3: Calorie restriction and BAM15 treatments improved whole-body blood glucose control. Blood glucose was measured prior to the start of treatment (pre-treatment) and after 4 weeks of treatment with BAM15 or calorie restriction (post-treatment). Intraperitoneal glucose tolerance test curves (A) and total area under the curve (AUC) (B). Blood glucose in the random fed state (AM) and after a 6-hour daytime fast (PM) (C). Plasma insulin levels in a random-fed state (AM) and after a 6-hour daytime fast (PM) (D). C-peptide (E) and proinsulin (F) concentrations in terminal sera. HOMA-IR as estimated from fasting glucose and insulin levels (G). Serum glucagon in terminal sera (H). * indicates $p < 0.05$ as assessed by Two-Way ANOVA with Dunnett's correction (B—D, G) or One-Way ANOVA (E, F, H). Graphs show mean ± SEM. n = 6—7 per group.

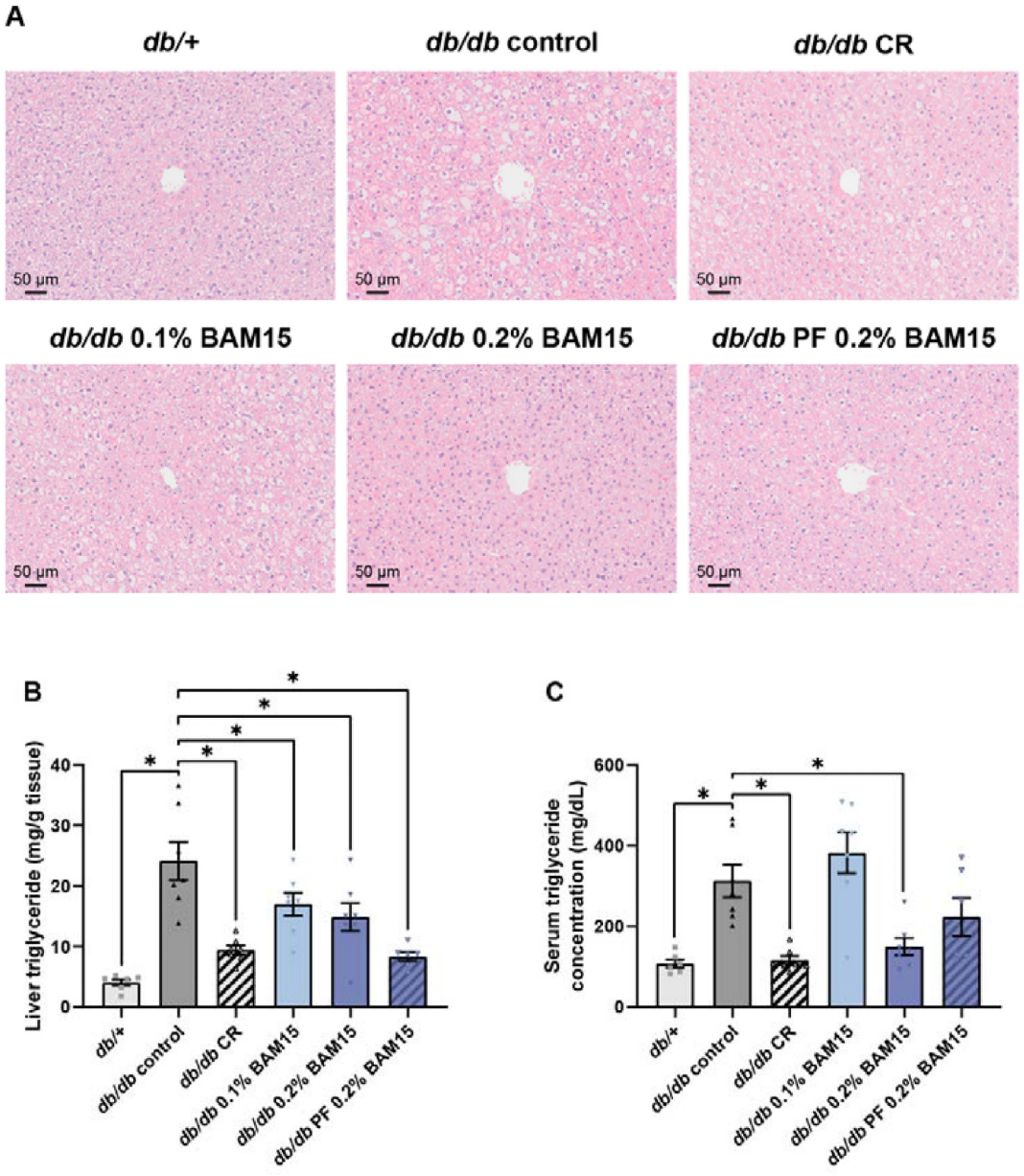

Figure 4: Calorie restriction and BAM15 treatments decreased liver and serum triglyceride concentrations. Representative images of liver sections stained with hematoxylin-eosin (A). Liver triglyceride content (B). Serum triglyceride content (C). * indicates $p < 0.05$ as assessed by One-Way ANOVA (B–C). All groups were compared to *db/db* controls. Graphs show mean ± SEM. n = 6–7 per group.

Glucagon, which opposes the actions of insulin, was approximately 2.5 times higher in the terminal sera of *db/db* control mice compared to *db/+* controls (94.8 ± 15.6 vs 38.4 ± 4.1 pg/mL) but was significantly decreased by 0.2% BAM15 *ad libitum* (50.4 ± 6.3 pg/mL), CR (36.4 ± 10.4 pg/mL) and 0.2% BAM15 pair-feeding (31.9 ± 9.7 pg/mL) (Figure 3H). Glucagon stimulates hepatic glycogenolysis while inhibiting glycogenesis; however, total liver glycogen content was not significantly altered among treatment groups (Fig. S8).

Immunohistochemistry showed a trend for increased beta-cell mass in *db/db* controls compared to *db/+* mice ($p = 0.051$), and significantly increased alpha-cell mass (Fig. S9). However, none of the treatments produced significant changes (Fig. S9). Based on immunofluorescent staining, there were also no statistically significant differences in the proportions of beta- vs alpha-cells among the groups (Figs. S10A–B), nor in the proportion of positive staining for Ki67, a marker for cell proliferation (Figs. S10C–D). The islet architecture in *db/db* control mice was visibly different to that of lean *db/+* mice, with more glucagon-positive cells in the center and less uniform insulin staining throughout (Fig. S10E). Islets from both 0.2% BAM15 treatment groups visually appeared more similar to *db/+* islets than *db/db* control islets (Fig. S10E).

3.5. Calorie restriction and BAM15 decreased liver steatosis

At study termination, liver and serum triglyceride content were determined. Fixed liver sections were stained with hematoxylin-eosin to visualize fatty change (Figures 4A, S11). Liver triglyceride levels were approximately 6 times higher in *db/db* control mice (24.2 ± 3.2 mg/g) compared to lean *db/+* controls (4.1 ± 0.5 mg/g) (Figure 4B).

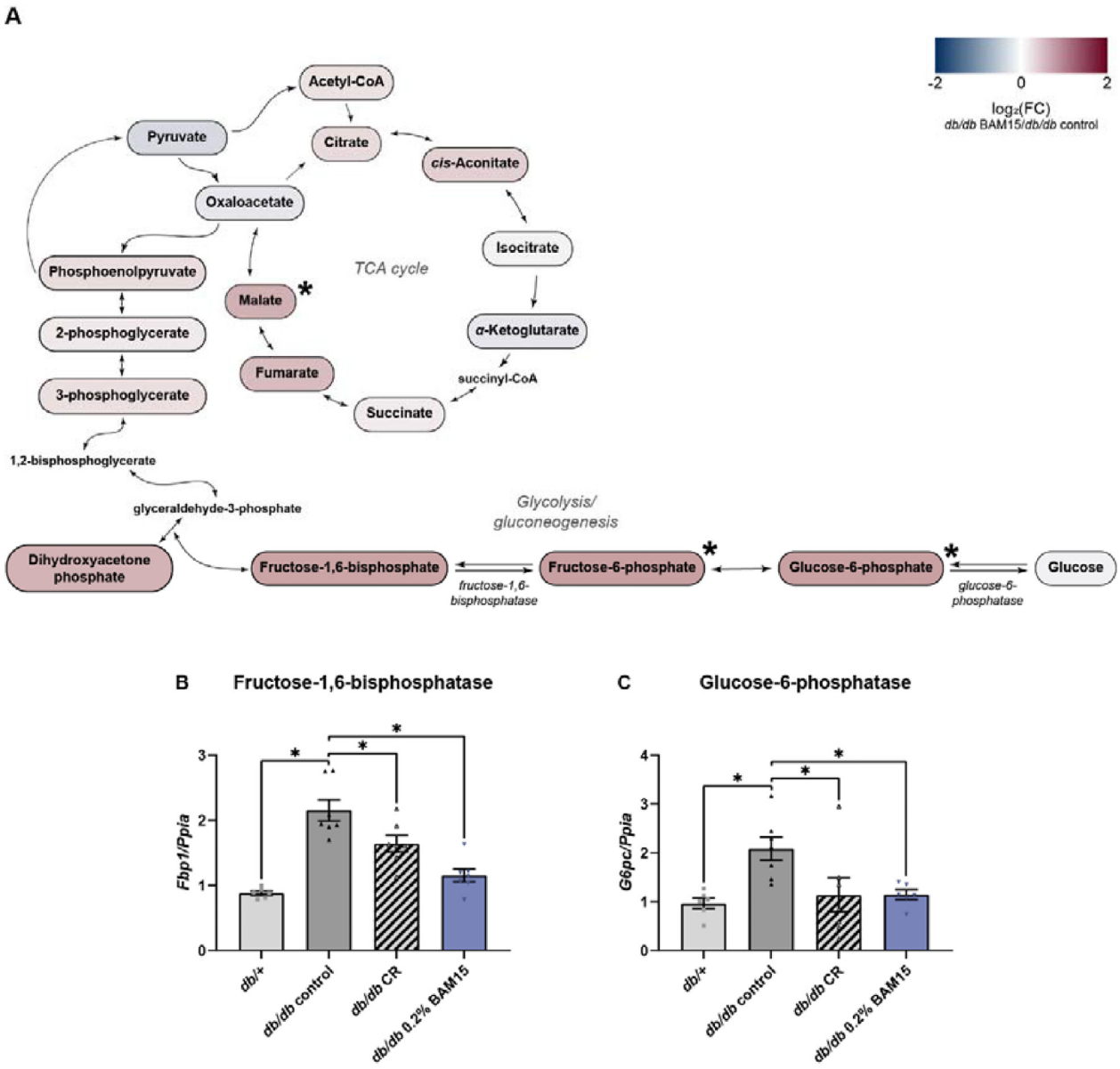

Figure 5: Metabolomic and gene expression analysis of liver tissue. Schematic showing key pathways for glucose metabolism (A). Metabolites are color-coded by $\log_2$ fold change of *db/db* 0.2% BAM15 compared to *db/db* control with increases shown in red and decreases shown in blue. Liver mRNA expression was measured in frozen tissue by qRT-PCR. Gene expression was measured for fructose-1,6-bisphosphatase (*Fbp1*, B) and glucose-6-phosphatase (*G6pc*, C). * indicates $p < 0.05$ as assessed by One-Way ANOVA. All groups were compared to *db/db* controls. Graphs show mean ± SEM. n = 6–7 per group.

Compared to *db/db* control mice, liver triglyceride content was decreased 61% by CR (9.4 ± 0.8 mg/g), 66% by pair-feeding 0.2% BAM15 (8.3 ± 0.8 mg/g), 38% by 0.2% BAM15 *ad libitum* (14.9 ± 6.2 mg/g), and 30% by 0.1% BAM15 *ad libitum* (17.0 ± 1.9 mg/g) (Figure 4B).

Serum triglyceride concentration was approximately three times higher in *db/db* control mice (313 ± 40.6 mg/L) compared to *db/+* mice (108 ± 10.0 mg/L) (Figure 4C). Compared to *db/db* control mice, calorie-restricted *db/db* mice had 63% less serum triglyceride (116 ± 10.3 mg/L), and mice fed *ad libitum* 0.2% BAM15 had 52% less serum triglyceride (150 ± 21.3 mg/dL), while the mice pair-fed 0.2% BAM15 had a non-statistically significant trend for lower serum triglyceride (224 ± 47 mg/dL) (Figure 4C). Serum triglyceride levels were unchanged by 0.1% BAM15 compared to *db/db* controls (Figure 4C). NEN treatment did not alter liver or serum triglyceride levels (Fig. S12).

3.6. BAM15 decreased the expression of genes encoding gluconeogenic enzymes

To investigate possible molecular mechanisms that mediate the glucose-lowering effects of BAM15, we conducted metabolomics analysis on frozen liver tissue of four treatment groups: *db/+*, *db/db* control, *db/db* CR and *db/db* 0.2% BAM15. The complete table of metabolites is provided as Supplementary Dataset 1, but the most relevant changes linking BAM15 treatment to the metabolic phenotype were observed in glucose metabolites and TCA cycle intermediates. A heatmap was constructed to show the changes in metabolite levels of *db/db* 0.2% BAM15 mice compared to *db/db* controls for the

glycolysis/gluconeogenesis pathway and the TCA cycle. BAM15 treatment increased levels of metabolites in the later stages of gluconeogenesis, such as dihydroxyacetone phosphate, fructose-1,6-bisphosphatase, fructose-6-phosphate and glucose-6-phosphate, with the latter two significantly increased ($p < 0.05$) and the former two showing a trend ($p = 0.07$) (Figure 5A). Fewer changes were detected in TCA cycle intermediates between *db/db* controls and 0.2% BAM15-treated mice with only malate being significantly increased in mice fed 0.2% BAM15.

Other altered metabolites include 1,5-anhydrosorbitol, which is a marker of glycemia and is decreased in humans with diabetes [24]. 1,5-anhydrosorbitol was significantly decreased in *db/db* controls compared to the other three groups (Supplementary Dataset 1). Betaine (trimethylglycine), a methyl group donor that has been implicated in improved glucose tolerance and decreased inflammation [25], was increased in *db/db* controls compared to *db/+* mice and CR- and BAM15-treated *db/db* mice (Supplementary Dataset 1). BAM15 also significantly increased concentrations of the primary bile acid cholate and secondary bile acid deoxycholate, and produced changes in metabolites involved in lysine degradation, such as 5-aminopentanoate, pipecholate, glutarate and 2-hydroxyglutarate (Supplementary Dataset 1).

Considering the significant accumulation of fructose-6-phosphate and glucose-6-phosphate, we next investigated the gene expression of key enzymes involved in gluconeogenesis. The gene expression of glucose-6-phosphatase (*G6pc*) and fructose-1,6-bisphosphatase (*Fbp1*), which catalyze rate-limiting steps in late-stage gluconeogenesis, were approximately two times higher in *db/db* control mice compared to *db/+* lean controls. Both CR and 0.2% BAM15 significantly decreased *G6pc* and *Fbp1* levels (Figure 5B–C). The lower *G6pc* and *Fbp1* expression in the liver tissue of 0.2% BAM15-treated mice is consistent with the observed increase in the concentrations of precursor substrates in the metabolomics data, including dihydroxyacetone phosphate, fructose-1,6-bisphosphatase, fructose-6-phosphate and glucose-6-phosphate (Figure 5A).

Overall, these data indicate that both CR and 0.2% BAM15 were able to decrease body weight, improve blood glucose control, and decrease liver triglyceride content. Specifically, CR and 0.2% BAM15 decreased body weight to a similar extent, but 0.2% BAM15 resulted in obviously greater improvements in glucose tolerance. The improvements in metabolism achieved by CR and 0.2% BAM15 were associated with decreased serum glucagon and decreased hepatic expression of enzymes catalyzing late-stage gluconeogenesis.

4. DISCUSSION

In this study, we observed that BAM15 treatment dose-dependently improved all measured hallmarks of metabolic disease in *db/db* mice, and generally outperformed both 50% calorie restriction and niclosamide ethanolamine. A major adverse phenotype in *db/db* mice is hyperglycemia and severe glucose intolerance. Compared to *db/db* controls, calorie-restricted *db/db* mice consumed 50% less food, weighed 24% less, and had a substantial but incomplete improvement in glucose tolerance. In this study, we found that low-dose 0.1% BAM15 resulted in a very similar improvement in glucose tolerance as 50% calorie restriction, but without any change in body weight or adiposity and despite consuming twice as much food. The most pronounced change in glucose homeostasis was observed in the two groups of *db/db* mice treated with 0.2% BAM15. These mice had body weights similar to 50% calorie-restricted mice, but completely normalized fed and fasted glucose levels and glucose tolerance similar to *db/+* mice. Therefore, 0.2% BAM15 produced superior improvements in glucose control than calorie restriction, but without decreasing food intake.

Plasma insulin levels were relatively unchanged among the *db/db* mice and only the 0.1% BAM15 group had an increase in fed insulin levels compared to *db/db* controls. Unexpectedly, HOMA-IR was increased in the 0.1% BAM15 group despite decreased blood glucose, indicating a compensatory increase in fasting insulin levels, even though the absolute values of fasting insulin were not statistically different from *db/db* controls. Although the increased insulin levels in the 0.1% BAM15 group suggested potential beta-cell compensation, no significant increase was observed in beta-cell mass, and C-peptide levels were not elevated in random-fed serum compared to *db/db* controls, which was similar to the results of CR treatment. It is possible that feeding activity immediately prior to collection of random-fed plasma samples could have caused an acute increase in fed insulin levels that was not reflected in the C-peptide values measured in random-fed terminal serum samples, especially because C-peptide has higher levels and longer half-life in circulation and would therefore be less affected by acute feeding behavior. Alternatively, CR and 0.1% BAM15 may have decreased the insulin clearance rate rather than impacting insulin secretion, consistent with previous literature showing that calorie restriction decreased the quantity of insulin-degrading enzyme in livers of *db/db* mice [26]. The potential effects of calorie restriction or a calorie restriction mimetic (such as uncoupling) on insulin clearance warrant further investigation in the future.

In contrast, the higher dose of 0.2% BAM15 decreased HOMA-IR compared to *db/db* controls, suggesting that this higher dose is able to induce sufficient improvements in insulin sensitivity to necessitate lower plasma insulin levels to control blood glucose. Treatment with 0.2% BAM15 also decreased proinsulin levels and C-peptide levels, which is consistent with the observed improvement in HOMA-IR and the implied decrease in insulin demand. However, the HOMA-IR values of all *db/db* groups remained higher compared to *db/+* control mice, indicating that none of the beneficial interventions were able to completely ameliorate insulin resistance despite lowering glucose levels and improving glucose clearance. Future studies involving hyperinsulinemic-euglycemic clamp experiments to measure insulin sensitivity may clarify the effects of insulin secretion and insulin action with each treatment.

Glucagon is the principal catabolic counter-regulatory hormone to insulin, acting on the liver to increase glucose output. Despite the lack of consistent change in insulin levels, we observed >2-fold hyperglucagonemia in *db/db* control mice that was nearly completely reversed by 50% calorie restriction and both 0.2% BAM15 treatments. Histologic examination determined that there were no changes in islet alpha- or beta-cell masses. Therefore, the changes in glucagon are likely to be due to altered glucagon secretion rather than alpha-cell abundance. In alpha-cells, glucagon secretion is regulated by a complex set of intrinsic and extrinsic factors, including nutrients, paracrine islet signaling, gut hormones, and the nervous system [27,28]. Our data suggest that treatment with calorie restriction and BAM15 can improve regulated glucagon secretion. Glucagon acts on the liver to increase hepatic glycogenolysis and gluconeogenesis, thus increasing hepatic glucose output [29]. Elevated glucagon levels and hepatic glucose output are important contributors to hyperglycemia in diabetes in people [30,31]; therefore, the lower blood glucagon concentration in the 50% calorie restriction- and BAM15-treated mice was likely an important mechanism for glucose control. Interestingly, in our study we observed that neither calorie restriction nor BAM15 altered total liver glycogen content. Liver glycogen in diabetic mice (*db/db*, NOD and

streptozotocin-induced) has been previously found to be more branched and prone to degradation than that of healthy mice, and this effect is associated with the loss of blood glucose homeostasis in diabetes [32–34]. Others have shown that improving blood glucose using certain traditional Chinese medicine compounds reverses the glycogen fragility in diabetic mice [35]. Therefore, we speculate that BAM15 may influence glycogen structural stability in a similar way, which would not have been detected in our measurement of total glycogen levels. Future investigations could shed further light on this possibility.

Both calorie restriction and BAM15 successfully decreased liver triglyceride content, consistent with the negative energy balance targeted by both treatments (by decreasing intake or increasing expenditure). Calorie restriction is associated with enhanced fatty acid oxidation and decreased *de novo* lipogenesis, leading to a net decrease in liver triglyceride content [16]. While hepatic steatosis is generally considered benign, it is strongly associated with poor glucose homeostasis and is a hallmark of non-alcoholic steatohepatitis, typically preceding the onset of inflammation and/or fibrosis [36]. Therefore, treatments that decrease liver fat are greatly desired.

In human patients, liver steatosis is correlated with insulin resistance and elevated hepatic glucose output, especially due to increased gluconeogenesis [37]. Therefore, the combination of reduced glucagon levels and decreased liver steatosis with 50% calorie restriction and 0.2% BAM15 treatment suggests that changes in hepatic glucose output could be important for the improved glucose control observed in these mice. A subset of treatment groups was selected to investigate relevant molecular mechanisms, including *db/+*, *db/db* control, *db/db* 50% calorie restriction, and *db/db* 0.2% BAM15. Metabolomics analysis showed that 0.2% BAM15-treated livers had increased dihydroxyacetone phosphate, fructose-1,6-bisphosphatase, fructose-6-phosphate and glucose-6-phosphate, which are the final metabolites in the gluconeogenesis pathway before glucose exits the cell. Consistent with the accumulation of metabolites late in the gluconeogenesis pathway, we also observed decreases in the gene expression of key enzymes that control late-stage gluconeogenesis in mice treated with 0.2% BAM15 and 50% calorie restriction, compared to *db/db* controls. These enzymes included fructose-1,6-bisphosphatase and glucose-6-phosphatase. Therefore, BAM15 and calorie restriction may restrict glucose efflux and create a bottleneck in the later stages of gluconeogenesis, thus lowering hepatic glucose output and improving blood glucose levels. However, we acknowledge the caveat that these inferences are drawn from metabolomics and gene expression data only, as we were unable to directly measure enzyme activity in frozen liver tissue.

In this study, one group of mice was fed 0.15% NEN in chow because this dose was previously shown to have anti-diabetic effects in *db/db* mice [17]. NEN is one of only two uncouplers that have previously been tested in *db/db* mice, the other being compound 6j [38]. However, as compound 6j was not commercially available, we selected NEN as an additional treatment group. Our NEN compound was effective *in vitro* in Seahorse Bioanalyzer assays but did not result in any differences in adiposity, blood glucose levels or plasma insulin levels in the *db/db* model when given at 0.15% (*w/w*) in food. Our results are consistent with another study that also failed to replicate the anti-diabetic properties of NEN at the same dose in the same mouse model [18]. NEN also failed to produce changes in liver steatosis and serum triglyceride content. Therefore, BAM15 outperformed NEN in all parameters measured. It is also worth noting that high-dose BAM15 resulted in superior phenotypes to those published for compound 6j in the context of fasting glucose, glucose tolerance, and liver triglyceride content in *db/db* mice [38].

This study has some limitations; for example, only male mice were used in this study. Future studies on female mice will provide greater translational relevance. In addition, as BAM15 has strong whole-body effects on metabolism, future work interrogating the molecular changes related to insulin sensitivity in diverse tissue types would be informative, although observational.

In summary, we observed that low-dose BAM15 treatment improved glucose homeostasis to a similar degree as ∼50% calorie restriction without altering food intake, body weight, or liver fat content. Meanwhile, high-dose BAM15 was very effective in correcting multiple defects associated with metabolic disease in *db/db* mice including liver triglyceride, glucose tolerance and body weight without causing a loss of lean muscle mass or decreasing food intake. Notably, the effect of high-dose BAM15 on glucose tolerance was superior to that of ∼50% calorie restriction. Taken together, the results of this study demonstrate the therapeutic potential of BAM15 for the treatment of metabolic disorders including diabetes.

AUTHOR CONTRIBUTIONS

Conceptualization: K.L.H, J.C.; Methodology: S,-Y.C., K.L.H.; Formal analysis: S.-Y.C., F.L.B.; Investigation: S.-Y.C., M.B., E.M.O., D.Y.H.W., S.J.A., D.P.S., I. A; Resources: J.M.S., C.J.G., B.J.C., K.A.R., G.C.S., W.L.S.; Writing — Original Draft: S.-Y.C., K.L.H.; Writing - Review & Editing: S.-Y.C., M.B., E.M.O., S.J.A., D.P.S., M.J.M., F.L.B., J.C., K.L.H.; Supervision: M.J.M., F.L.B., K.L.H.

DISCLOSURES

K.L.H. and W.L.S. declare equity interest in Life Biosciences Inc. All other authors have no conflicts of interest.

DATA AVAILABILITY

Data will be made available on request.

ACKNOWLEDGEMENTS

We thank Peter Geelan-Small and Eve Slavich (Stats Central, UNSW) for guidance with statistics. EchoMRI data presented in this work were acquired using instruments at the Biological Resources Imaging Laboratory, LC-MS/MS data were acquired using instruments at the Bioanalytical Mass Spectrometry Facility, and histological data were acquired using instruments at the Katharina Gaus Light Microscopy Facility, within the Mark Wainwright Analytical Centre (MWAC) of UNSW Sydney, which is in part funded by the Research Infrastructure Programme of UNSW. Metabolomics data was obtained using NCRIS-enabled Metabolomics Australia infrastructure at the University of Melbourne and funded through BioPlatforms Australia. This work was supported by a National Health and Medical Research Council (NHMRC) Ideas Grant (GNT2011004) to K.L.H. and a US National Institutes of Health (NIH) RO1 Grant to W.L.S. and K.L.H. (DK128612). S.-Y.C., S.J.A. and D.P.H. are supported by UNSW Scientia PhD Scholarships. F.L.B is supported by a Cancer Institute NSW Career Development Fellowship (2021/CDF1120).

CONFLICT OF INTEREST

None declared.

APPENDIX A. SUPPLEMENTARY DATA

Supplementary data to this article can be found online at https://doi.org/10.1016/j.molmet.2023.101684.

REFERENCES

[1] Jaacks LM, Vandevijvere S, Pan A, McGowan CJ, Wallace C, Imamura F, et al. The obesity transition: stages of the global epidemic. Lancet Diabetes Endocrinol 2019;7(3):231–40.

[2] IDF. IDF diabetes atlas 10th edition. In: Boyko EJ, Magliano DJ, Karuranga S, Piemonte L, Riley P, Saeedi P, et al., editors. IDF diabetes atlas. Brussels, Belgium: International Diabetes Federation; 2021. https://www.diabetesatlas.org.

[3] Younossi Z, Anstee QM, Marietti M, Hardy T, Henry L, Eslam M, et al. Global burden of NAFLD and NASH: trends, predictions, risk factors and prevention. Nat Rev Gastroenterol Hepatol 2018;15(1):11–20.

[4] Ortega FB, Lavie CJ, Blair SN. Obesity and cardiovascular disease. Circ Res 2016;118(11):1752–70.

[5] Lauby-Secretan B, Scoccianti C, Loomis D, Grosse Y, Bianchini F, Straif K. Body fatness and cancer–viewpoint of the IARC working group. N Engl J Med 2016;375(8):794–8.

[6] Mazon JN, de Mello AH, Ferreira GK, Rezin GT. The impact of obesity on neurodegenerative diseases. Life Sci 2017;182:22–8.

[7] Kwok S, Adam S, Ho JH, Iqbal Z, Turkington P, Razvi S, et al. Obesity: a critical risk factor in the COVID-19 pandemic. Clin Obes 2020;10(6):e12403.

[8] Redman LM, Heilbronn LK, Martin CK, de Jonge L, Williamson DA, Delany JP, et al. Metabolic and behavioral compensations in response to caloric restriction: implications for the maintenance of weight loss. PLoS One 2009;4(2):e4377.

[9] Goedeke L, Shulman GI. Therapeutic potential of mitochondrial uncouplers for the treatment of metabolic associated fatty liver disease and NASH. Mol Metabol 2021;46:101178.

[10] Childress ES, Alexopoulos SJ, Hoehn KL, Santos WL. Small molecule mitochondrial uncouplers and their therapeutic potential. J Med Chem 2018;61(11):4641–55.

[11] Merry BJ. Oxidative stress and mitochondrial function with aging – the effects of calorie restriction. Aging Cell 2004;3(1):7–12.

[12] Walsh ME, Shi Y, Van Remmen H. The effects of dietary restriction on oxidative stress in rodents. Free Radic Biol Med 2014;66:88–99.

[13] Burke SJ, Batdorf HM, Burk DH, Noland RC, Eder AE, Boulos MS, et al. Db/db mice exhibit features of human type 2 diabetes that are not present in weight-matched C57BL/6J mice fed a Western diet. J Diabetes Res 2017;2017:8503754.

[14] Dalboge LS, Almholt DL, Neerup TS, Vassiliadis E, Vrang N, Pedersen L, et al. Characterisation of age-dependent beta cell dynamics in the male db/db mice. PLoS One 2013;8(12):e82813.

[15] Ishida E, Kim-Muller JY, Accili D. Pair feeding, but not insulin, phloridzin, or rosiglitazone treatment, curtails markers of β-cell dedifferentiation in db/db mice. Diabetes 2017;66(8):2092–101.

[16] Kim KE, Jung Y, Min S, Nam M, Heo RW, Jeon BT, et al. Caloric restriction of db/db mice reverts hepatic steatosis and body weight with divergent hepatic metabolism. Sci Rep 2016;6(1):30111.

[17] Tao H, Zhang Y, Zeng X, Shulman GI, Jin S. Niclosamide ethanolamine-induced mild mitochondrial uncoupling improves diabetic symptoms in mice. Nat Med 2014;20(11):1263–9.

[18] Hinder LM, Sas KM, O'Brien PD, Backus C, Kayampilly P, Hayes JM, et al. Mitochondrial uncoupling has no effect on microvascular complications in type 2 diabetes. Sci Rep 2019;9(1):881.

[19] Alexopoulos SJ, Chen S-Y, Brandon AE, Salamoun JM, Byrne FL, Garcia CJ, et al. Mitochondrial uncoupler BAM15 reverses diet-induced obesity and insulin resistance in mice. Nat Commun 2020;11(1):2397.

[20] Folch J, Lees M, Sloane Stanley GH. A simple method for the isolation and purification of total lipides from animal tissues. J Biol Chem 1957;226(1):497–509.

[21] Byrne FL, Olzomer EM, Brink R, Hoehn KL. Knockout of glucose transporter GLUT6 has minimal effects on whole body metabolic physiology in mice. Am J Physiol Endocrinol Metabol 2018;315(2):E286–93.

[22] Grubbs FE. Procedures for detecting outlying observations in samples. Technometrics 1969;11(1):1–21.

[23] Chen S-Y, Beretta M, Alexopoulos SJ, Shah DP, Olzomer EM, Hargett SR, et al. Mitochondrial uncoupler SHC517 reverses obesity in mice without affecting food intake. Metabolism 2021:154724.

[24] Dungan KM. 1,5-anhydroglucitol (GlycoMark) as a marker of short-term glycemic control and glycemic excursions. Expert Rev Mol Diagn 2008;8(1):9–19.

[25] Zhao G, He F, Wu C, Li P, Li N, Deng J, et al. Betaine in inflammation: mechanistic aspects and applications. Front Immunol 2018;9:1070.

[26] Nonaka Y, Takeda R, Kano Y, Hoshino D. Short-term calorie restriction maintains plasma insulin concentrations along with a reduction in hepatic insulin-degrading enzyme levels in db/db mice. Nutrients 2021;13(4):1190.

[27] Albrechtsen NJW, Kuhre RE, Pedersen J, Knop FK, Holst JJ. The biology of glucagon and the consequences of hyperglucagonemia. Biomarkers Med 2016;10(11):1141–51.

[28] Andersen DB, Holst JJ. Peptides in the regulation of glucagon secretion. Peptides 2022;148:170683.

[29] Jiang G, Zhang BB. Glucagon and regulation of glucose metabolism. Am J Physiol Endocrinol Metabol 2003;284(4):E671–8.

[30] Matsuda M, DeFronzo RA, Glass L, Consoli A, Giordano M, Bressler P, et al. Glucagon dose-response curve for hepatic glucose production and glucose disposal in type 2 diabetic patients and normal individuals. Metab, Clin Exp 2002;51(9):1111–9.

[31] Baron AD, Schaeffer L, Shragg P, Kolterman OG. Role of hyperglucagonemia in maintenance of increased rates of hepatic glucose output in type II diabetics. Diabetes 1987;36(3):274–83.

[32] Deng B, Sullivan MA, Li J, Tan X, Zhu C, Schulz BL, et al. Molecular structure of glycogen in diabetic liver. Glycoconj J 2015;32(3):113–8.

[33] Hu Z, Li E, Sullivan MA, Tan X, Deng B, Gilbert RG, et al. Glycogen structure in type 1 diabetic mice: towards understanding the origin of diabetic glycogen molecular fragility. Int J Biol Macromol 2019;128:665–72.

[34] Li C, Hu Z. Is liver glycogen fragility a possible drug target for diabetes? FASEB J 2020;34(1):3–15.

[35] Li C, Gan H, Tan X, Hu Z, Deng B, Sullivan MA, et al. Effects of active ingredients from traditional Chinese medicines on glycogen molecular structure in diabetic mice. Eur Polym J 2019;112:67–72.

[36] Nassir F, Rector RS, Hammoud GM, Ibdah JA. Pathogenesis and prevention of hepatic steatosis. Gastroenterol Hepatol 2015;11(3):167–75.

[37] London A, Lundsgaard AM, Kiens B, Bojsen-Møller KN. The role of hepatic fat accumulation in glucose and insulin homeostasis-dysregulation by the liver. J Clin Med 2021;10(3).

[38] Jiang H, Jin J, Duan Y, Xie Z, Li Y, Gao A, et al. Mitochondrial uncoupling coordinated with PDH activation safely ameliorates hyperglycemia via promoting glucose oxidation. Diabetes 2019;68(12):2197–209.

